

A Low-Power Neuromorphic Approach for Efficient Eye-Tracking

Pietro Bonazzi¹, Sizhen Bian¹, Giovanni Lippolis², Yawei Li¹, Sadique Sheik³, Michele Magno¹
¹ETH Zürich, ²Inivation AG, ³Synsense AG

Abstract

This paper introduces a neuromorphic methodology for eye tracking, harnessing pure event data captured by a Dynamic Vision Sensor (DVS) camera. The framework integrates a directly trained Spiking Neuron Network (SNN) regression model and leverages a state-of-the-art low power edge neuromorphic processor - Speck, collectively aiming to advance the precision and efficiency of eye-tracking systems. First, we introduce a representative event-based eye-tracking dataset, "Ini-30," which was collected with two glass-mounted DVS cameras from thirty volunteers. Then, a SNN model, based on Integrate And Fire (IAF) neurons, named "Retina", is described, featuring only 64k parameters (6.63x fewer than the latest) and achieving pupil tracking error of only 3.24 pixels in a 64x64 DVS input. The continuous regression output is obtained by means of convolution using a non-spiking temporal 1D filter slid across the output spiking layer. Finally, we evaluate Retina on the neuromorphic processor, showing an end-to-end power between 2.89-4.8 mW and a latency of 5.57-8.01 mS dependent on the time window. We also benchmark our model against the latest event-based eye-tracking method, "3ET", which was built upon event frames. Results show that Retina achieves superior precision with 1.24px less pupil centroid error and reduced computational complexity with 35 times fewer MAC operations. We hope this work will open avenues for further investigation of close-loop neuromorphic solutions and true event-based training pursuing edge performance.

Reproducibility

<https://github.com/pbonazzi/retina>

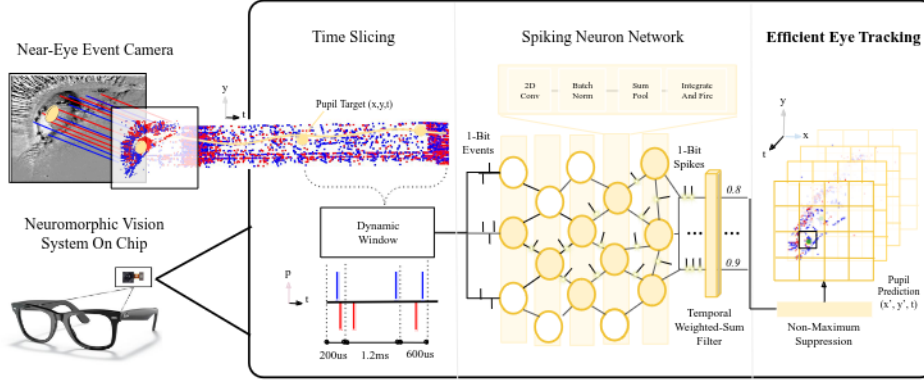
Acknowledgments

This research was funded by Innosuisse (103.364 IP-ICT). We thank Wolfgang Böttcher, Adam Radomski and Nogay Küpelioğlu for the great help during the collection of the Ini-30 dataset and the Deployment on Speck.

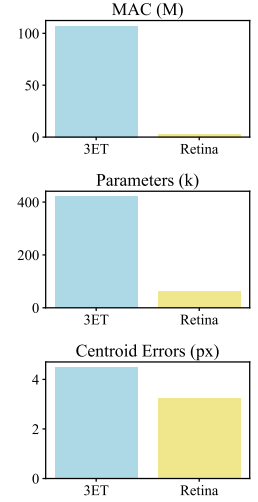
1. Introduction

Neuromorphic systems, mimicking the neurobiological architectures of the human brain, have emerged as a promising paradigm for sensory processing [2, 16]. An example of those are event cameras and spike-based computation, which present distinctive advantages compared to traditional frame-based cameras and Artificial Neuron Network (ANN). These benefits encompass heightened energy efficiency and decreased computing complexity. In the context of neuromorphic systems for eye tracking, various challenges confront the field. First, even the most recent methods either rely on frame-based input [5, 25] or focus on end-to-end tasks, such as gaze tracking learned from screen-level coordinates [1]. However, pupil tracking serves as a crucial initial phase in the gaze estimation pipeline. When mastered, it can facilitate applications to extend their capabilities beyond controlled environments. Second, state-of-the-art algorithms for event-based eye tracking are model-based and require subject-specific calibration [1, 25] and fitting at the moment of use, limiting their practicality in certain applications like consumer AR/VR technology [24]. Eye-tracking algorithms and systems demand a nuanced equilibrium and trade-off between resolution, frame rate, latency and power consumption, as each pixel carries energy and bandwidth costs during the acquisition process. To overcome this challenge, sophisticated eye-tracking systems utilize high-speed event-based cameras, necessitating innovative algorithms and processing units capable of harnessing the event-driven nature of this new camera technology [1]. One of the most recent papers on event-based eye tracking without subject-dependent calibration was authored by Chen et al. [5]. Notably, in this work, they accumulated and normalized synthetically generated events to a 32-bit frame for its input. This approach is inefficient as it does not leverage the asynchronous 1-bit nature of the event data. Finally, there is a need for end-to-end assessments of neuromorphic System-on-Chip (SoC) platforms in terms of power consumption and latency, with the object of informing the design of efficient machine learning algorithms, that leverage event input and spike-based computation [4, 18].

To address these challenges, we propose an eye-tracking model, dubbed "Retina", suitable for deployment on a neu-



(a) Architectural overview of the proposed method.



(b) Key results.

Figure 1. The processing pipeline of our method. Event-based efficient eye tracking is achieved by training a spiking neural network on our proposed dataset and deploying it on a neuromorphic System-on-Chip (SoC).

romorphic asynchronous SoC, Synsense Speck (Speck). We leverage spike-based computation and real event input to offer energy-efficient eye tracking of the pupil from near-eye events. In detail, our work introduces the following three key contributions:

1. **Event-based Eye Tracking Dataset, "Ini-30"**: We introduce a representative event-based eye-tracking dataset, named "Ini-30". Our dataset is collected with two event cameras mounted on a glass frame, and features variable recording lengths and event counts from 30 volunteers, providing an ideal benchmark for modeling the heterogeneity of event-based eye tracking in real-world scenarios. Considering the variability of the dataset, we slice the event data based on quantity of events instead of fixed timestamps. This method enables domain gap adaptation between different DVS, solves the difference in temporal event growth between real recordings, and allows constant input to be processed by the model at every timestamp.
2. **Event-based Eye Tracking Algorithm, "Retina"**: Retina is a SNN structure based on IAF neurons, followed by a non-spiking temporal weighted-sum filter for regression, which converts spikes to bounding box predictions. The filter allows IAF neurons to learn temporal information without having to fall back to a voltage decay factor [4] or recurrent neurons, which are not supported in the tested hardware, Speck. Our work shows superior precision (~20% centroid error) and reduced computational complexity (~30x MAC) against the existing latest event-based eye tracking method, "3ET" [5].
3. **Deployment on Neuromorphic Hardware**: Finally,

we deploy our model on an "edge" neuromorphic SoC, Speck, and provide power and latency results for network inference using injected events and end-to-end evaluations by activating the on-board DVS camera.

2. Related Work

This section discusses the state-of-the-art explorations of eye-tracking based on a comprehensive literature survey. Depending on the utilized signal form (non-event or event input), we separate the existing eye-tracking solutions into two approaches:

2.1. Non-Event-Based Eye Tracking

Conventional non-event-based eye-tracking includes model-based and appearance-based methods. The former one either tracks specular glint reflections for corneal curvature center detection [8, 20], or extracts salient geometrical features of the eye from frames and tracks the pupil with an optimized fitting method based on a physics eye model [10, 21]. Such an approach commonly supplies impressive tracking accuracy, achieving sub-degree tracking error [12], while stunted by the deployment complexity, such as ambient light conditions, image resolution, and calibration requirement. The latter one typically applies a trained machine-learning model to the raw eye images for tracking [3, 9, 15, 24]. This approach gives an end-to-end, deployable eye-tracking solution, which is heavily limited by the frame rate of the camera, with resulting tracking rate that can reach a maximum of 300 Hz. Differently from this line of work, the event-based eye tracking can reach

Table 1. A summary of the related work in event-based pupil/gaze tracking

Year-Work	DVS Camera	Dataset	Input	Algorithm	Event Rate	Energy	Precision
2020-[1]	DAVIS346b	Customized	Frames/Events	Model-based	$\geq 10\text{ KHz}$	N/A ^a	$0.45^\circ\text{--}1.75^\circ$
2022-[19]	Prophesee G3.1	N/A	Events/LED Markers	Glint Detection	1 KHz	$\approx 35\text{ mW}^b$	$< 0.5\text{px}$
2023-[25]	DAVIS346	EV-Eye	Frames/Events	Point2Edge	$\leq 38.4\text{ KHz}$	N/A	$1.2\text{--}7.7\text{px}$
2023-[5]	N/A	Synthetic	Event-frames	ConvLSTM	95 KHz	N/A	N/A
Ours	DVXplorer	Ini-30	Events	SNN	$\leq 5\text{ KHz}^c$	$2.89^d\text{--}4.8\text{ mW}^d$	$3\text{--}8\text{px}$

^a Not Available.^b Sensor power only.^c Depending on the DVS and time window length.^d End-to-end power.

beyond kHz [1] of update rate and provide energy-efficient observations [6].

2.2. Event-Based Eye Tracking

Benefiting from the sparse event stream and high dynamic range of event cameras, event-based eye-tracking has emerged as a groundbreaking solution enabling beyond- kHz and low-power consumption eye-tracking, as listed in Tab. 1. The first event-based eye-tracking work was published in 2020 [1], in which the authors proposed a hybrid frame-event-based near-eye gaze tracking system offering update rates beyond 10 kHz with an accuracy comparable to commercial tracker. The algorithm is based on a parametric pupil model and utilizes the event to update the model with a pupil-fitting method. This work is sensitive to sensor noises, as choosing the useful event that can be used to update the model is challenging. Following this work, researchers have published another three event-based pupil/gaze-tracking papers in the past three years. Stoffregen et al. [19] described the first fully event and model-based glint tracker, which is robust to background disturbances and has a sampling rate of 1 kHz with an estimated power of 35 mW (sensing components only). Here the author used coded differential lighting to enhance the glint detection with an event camera. Similar to [1], in [25], the authors presented a hybrid eye-tracking method that leverages both the near-eye grayscale images and event data for robust and high-frequency eye tracking. The proposed matching-based pupil tracking method gave a pixel error of only 1.2 px with a peak tracking frequency of up to 38.4 kHz . In [5], the authors proposed a sparse change-based convolutional Long-Short-Term-Memory (LSTM) model for event-based eye tracking, which reduces arithmetic operations by approximately $4.7\times$, compared to a standard convolutional LSTM, without losing accuracy when tested on a synthetic event dataset.

There are several limitations to existing methods. First, they rely on frames, either directly from the sensor output [1, 25],

which decreases the power efficiency of the system, or accumulate the events into frames and process the frames with deep neural network [5], which sacrifices the temporal resolution, introduces latency and increase the memory footprint. Second, with a purely event-based solution, auxiliary devices are used to enhance specular events [19]. Besides that, none of the existing works carried out a real deployment of their proposals, especially on a neuromorphic platform that perfectly matches the sparsity of the event stream. Thus, the system-level performance in the energy and latency that an event solution can bring is still unclear. In contrast, our work presents a SNN supported by an end-to-end neuromorphic edge system leveraging pure events stream from a DVS camera.

3. Dataset

Several prominent eye-tracking and gaze estimation datasets have contributed significantly to the advancement of this field using frame cameras [11, 23]. To the best of our knowledge, the only available event-based datasets have been presented by Angelopoulos et al. [1] for *gaze tracking* and in Zhao et al. [25] for *gaze and eye tracking*. In this paper, we introduce a representative event-based *eye tracking* dataset, dubbed "Ini-30", which, differently from EV-Eye [25], was collected with two event cameras (one per eye) mounted on a glass-frame instead of in a controlled environment.

3.1. Dataset Collection

The Ini-30 dataset is collected with two event cameras mounted on a glass frame. Each DVXplorer sensor (640×480 pixels) is attached on the side of the frame. During data collection, the participants looked around the room and walked a few steps. As shown in Fig. 2, the event cameras are securely screwed on a 3D-printed case attached to the side of the glass frame. We labeled the position of the pupil in the DVS's array manually, using an assistive label-

ing tool. The number of labels per recording spans from 475 to 1'848 and time per label ranges from 20.0 to 235.77 milliseconds depending on the overall duration of the sample.

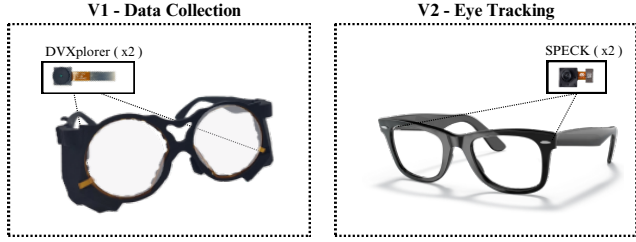


Figure 2. A picture of the hardware for data collection (v1) and the future design of eye tracking on-glass (v2).

This setup allows for unconstrained head movements, enabling the capture of event data due to eye movement in a naturalistic setting and thus allowing us to generate a real, diverse and challenging dataset. In the next section, we characterize the dataset and define it in comparison with other event-based datasets.

3.2. Dataset Characterization

In this section, we present a comparative analysis of the dataset presented in Angelopoulos [1] and our proposed Ini-30 dataset, which are summarized in Tab. 2. To the best of our knowledge, Ini-30 is the first eye-tracking event-based dataset with pupil location labelled on the sensor. The other dataset [1, 25] consist of screen point coordinates (x, y) , instead of pupil location coordinates (x, y) on the DVS's array. Labeling pupil locations provides superior precision and granularity for understanding gaze behavior compared to screen coordinates. Our approach offers robustness to head movements, dynamic adaptation to display changes, more insights to enhancing the efficacy of gaze tracking.

Table 2. Comparison between our proposed dataset (Ini-30) with the one proposed by Angelopoulos [1].

Aspect	Angelopoulos [1]	Ini-30 (Ours)
Annotations	Screen Coord.	Pupil Coord.
Sensors	DAVIS346b	DVXplorer
Resolution	346×260 px	640×480 px
NIR Illumination	Yes	Yes
User's Head	Fixed (head rest)	Unconstrained
Camera Loc.	On Desk	On Glass
Recordings	54	30
Variability*	Low	High

* Variability refers to the difference in duration of each recordings and the temporal growth trend of event counts within recordings.

Angelopoulos [1] employs DAVIS346b (346×260 px), whereas our Ini-30 dataset incorporates DVXplorer sensor,

providing enhanced visual fidelity at 640×480 px. Both datasets are collected using Near-Infra Red (Illumination) (NIR) illumination technology, to highlights the events surrounding the pupil. Additionally, Angelopoulos [1] captures subjects with fixed head positions, while Ini-30 is designed for use cases with unconstrained head movements with cameras mounted directly on glass frames. Because of this, Ini-30 covers a broader range of situations. Temporally, Angelopoulos [1] maintains fixed recording lengths (30s) and linearly growing event counts, while Ini-30 showcases richer variability, with recording durations ranging from 14.64 to 193.8 seconds.

Tab. 3 provides key statistics for Ini-30, in the context of event cameras updates rates. The sampling time step ranges from 61 to 346 microseconds, and the event count per timestep spans from 3 to 5'000 events.

Table 3. Event cameras updates rates (T_s [μs]) in Ini-30.

Name	Median	Mean	Std	Min	Max
T_s [μs]	200	200	14	61	346
Events / T_s	94	175	299	3	4'799

Overall, our dataset encompasses a diverse range of recordings (30), with labels per recording spanning from 475 to 1'848, with total event data varying from 4.8 million to 24.2 million, and time per label ranging from 20.0 to 235.77 milliseconds. This information helped informed data preparation strategies in our models which consider a temporal dimension.

4. Methodology

We propose a low latency and lightweight architecture and learning rule for an eye-tracking algorithm based on event data. Our network is a single SNN featuring spiking spatial convolutions and fusible batch normalization layers. The spiking outputs are converted to continuous values by means of a 1D convolution layer with fixed weights. An overview of our network configurations can be found in Tab 5, while other implementation details are described in the next subsections.

4.1. Data Preparation

Since the algorithm is deployed on the neuromorphic SoC Speck, which has two-channel support for a 64×64 DVS's resolution, we prepared the dataset to bridge this domain gap. First, we transformed the rectangular resolution of the original data to a squared array of 512×512 , by shifting the y-axis to 16 pixels and discarding 128 X-coordinates in correspondence to the spatial location where fewer events are present and no label appeared ($x < 96$ and $x > 608$). Next,

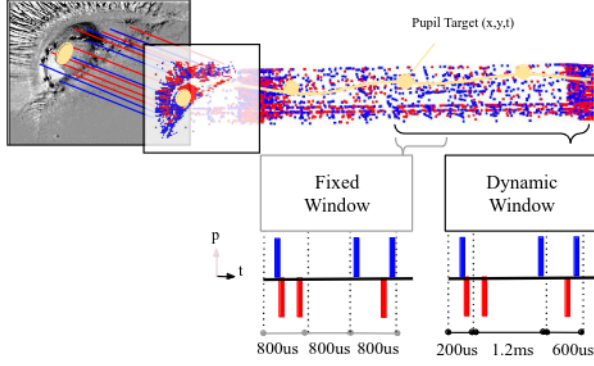
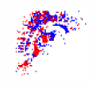
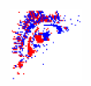
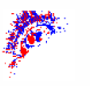
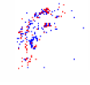
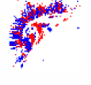
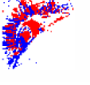


Figure 3. A graph illustrating the different techniques for slicing events (red, blue) in time: A) $dt = 800\mu s$, B) events count = 2.

we applied sum pooling to reach the Speck compatible resolution and proceeded to dynamically slice the event temporally. Every video was sliced, from a point in time corresponding to a pupil label timestamp, until we obtained a desired pixel activations. This results in better input data for convolution layers, (Tab. 4), Fig. 3 shows an illustrated example of the working principles of the two techniques. In case multiple events from the same pixels are found during this slicing step, we keep the event polarity with the highest number of events and then clip the event frame back to 0 and 1, ensuring only one channel is active at every timebin. Finally, since in our dataset, the sampling time of events has a median of $200\mu s$, Tab. 3, while pupil labels have a frequency of around $30ms$, we weight-interpolated new labels at bin time using the two closest labels in the source recordings. We trained our network with 64 timebins, shuffling each slice of recording only during training.

Table 4. An example of the qualitative improvements of 1) dynamic time window compared to 2) fixed time.

Method	t	t_{i+1}	t_{i+2}
1)			
2)			

4.2. Network Architecture

After the data preparation step, events are processed sequentially at fixed timestamps by kernel of the convolution, batch normalization layers and IAF neurons in our model. We designed each layer of our network to fit the memory

limitation of the available cores in the targeted platform, Speck.

We computed the total kernel memory available K_{MT} for each layer following the basic formula:

$$K_{MT} = c2^{\log_2 k_x k_y + \log_2 f} \quad (1)$$

Where c is the input channel of M , f is the output channel number, k_x and k_y are the kernel size. The necessary neuron memory N_M entries are computed by solving the following formulas:

$$N_M = f f_x f_y \quad (2)$$

Where f is the output channel number and f_x and f_y depend on the input feature map size c_x , c_y , stride s_x , s_y , and padding p_x , p_y , following the relationships:

$$f_x = \frac{c_x - k_x + 2p_x}{s_x} + 1, f_y = \frac{c_y - k_y + 2p_y}{s_y} + 1 \quad (3)$$

In Tab. 5, we present an overview of the network. The events are processed by Layer ID "1" and sequentially transmitted to the following layers. Every convolution operation is followed by a spiking neuron with a spiking threshold of 1 and a minimum voltage membrane of -1. Given that spike generation is non-differentiable, we use a surrogate gradient [14] periodic exponential function [22].

The spikes generated by the final layer are converted to continuous values using a 1-dimensional non-spiking temporal weighted-sum filter with fixed weights, discussed in Sec. 4.3. Next, akin to other grid-based methodologies such as those presented by Redmon et al. [17], we modify the output layer to consist of 4×4 cells, each containing two 5-dimensional vectors representing the top right and bottom left coordinates of the bounding box, along with a confidence score. To refine the bounding box localization, we employ a post-processing step using Non-Maximum Suppression (NMS) [7], which helps eliminate redundant detections by retaining only the highest-scoring bounding boxes while discarding overlapping alternatives. In section Sec. 4.4, we present how we compare the prediction to a generated target bounding box synthetically generated around the original 1-pixel label by expanding it to 2 pixels in each direction.

4.3. Temporal Weighted-Sum Filter

The implemented temporal weighted-sum filter can be described as follows:

$$y(t) = \sum_{i=1}^N w_i \cdot x(t-i) \quad (4)$$

where $y(t)$ represents the filtered output at time t , N is the length of the convolutional kernel, w_i denotes the filter

Table 5. The network configuration, memory footprint and core compatibility on Speck for each layer.

Layer ID	SNN	c_{in}	c_{out}	$k_x * k_y$	$s_x * s_y$	N_M	K_{MT}	Cores ID
1	BatchConv IAF Pool	2	16	5×5 2×2	2×2 1×1	0.78 KiB	15.02 KiB	all
2	BatchConv IAF Pool	16	64	3×3 2×2	1×1 1×1	9.00 KiB	64.00 KiB	0, 1, 2
3	BatchConv IAF Pool	64	16	3×3 2×2	1×1 1×1	9.00 KiB	4.00 KiB	all
4	BatchConv IAF	16	16	3×3	1×1	2.25 KiB	1.00 KiB	all
5	BatchConv IAF	16	8	3×3	1×1	1.12 KiB	0.50 KiB	all
6	BatchConv IAF	8	16	3×3	1×1	1.12 KiB	1.00 KiB	all
7	BatchConv IAF	144	128	1×1	1×1	18.00 KiB	1.12 KiB	3, 4, 5, 6
8	BatchConv IAF	128	160	1×1	1×1	34.37 KiB	2.42 Ki	5, 6

weight at position i in the kernel, and $x(t - i)$ is the input value at time $t - i$.

The filter weights (w_i) are determined by a 'synaptic kernel' $S(t)$ and 'membrane kernel' $M(t)$, which in turn are computed based on a membrane constant (τ_{mem}) and a synaptic constant (τ_{syn}):

$$S(t) = \exp\left(-\frac{t}{\tau_{syn}}\right), M(t) = \exp\left(-\frac{t}{\tau_{mem}}\right) \quad (5)$$

The membrane kernel initializes the weights of a 1D convolution applied to the synaptic kernel. The weights w_i of the temporal weighted-sum filter w_i are initialized as a result of the synaptic and membrane kernel convolution.

4.4. Loss Function

Our loss function \mathcal{L} is a combination of several components: a box loss \mathcal{L}_{box} , a confidence loss \mathcal{L}_{conf} , a synaptic loss \mathcal{L}_{syn} .

The box loss \mathcal{L}_{box} measures how well the model can localize the pupil within the image, by minimizing the mean squared error distance between the predicted p_i and target t_i bounding boxes, represented as:

$$\mathcal{L}_{box} = \sum_{i=1}^N (p_i - t_i)^2 \quad (6)$$

The confidence loss \mathcal{L}_{conf} measures how confident the model is about its prediction, by penalizing low confidence scores for correct predictions and high confidence scores for incorrect predictions. This component is calculated as a mean squared error distance between the predicted and target confidence scores (c_i and g_i):

$$\mathcal{L}_{conf} = \sum_{i=1}^N (c_i - g_i)^2 \quad (7)$$

The synaptic loss \mathcal{L}_{syn} is the first of our regularization terms and it ensures that the number of multiply-accumulate operations performed by the neurons in the network at each layer is within a range the neuromorphic SoC Speck can handle (1e6). \mathcal{L}_{syn} is formulated as the squared difference between the target synaptic operations with each layer synaptic operations, normalized by the square of the target synaptic operations. The total loss \mathcal{L} is a weighted sum of these components. To summarize, the \mathcal{L}_{box} and \mathcal{L}_{conf} are tasks losses which are used to detect the pupil in the event array. The \mathcal{L}_{syn} is a regularization component in order to deploy the network on the neuromorphic device.

5. Experiments

5.1. Setup

Our precision results are based on the actual centroid error in pixels extracted from the predicted bounding box. We

evaluated the efficiency of our algorithm by measuring the power (P) [mW] consumption on the neuromorphic SoC and by counting the number of parameters and Multiply and Accumulate (MAC) operations. Regarding our implementation, we trained every convolution layer M with 8-bit weight parameters (kernel memory K_{MT}) and a 16-bit spiking neuron states (neuron memory N_M). Batch normalization layers are fused to the convolution blocks in inference. The models are trained for 576 iterations using the ADAM optimizer and a step learning rate scheduler with a gamma of 0.8. Furthermore, we reset the states of the neuron at every iteration only during training. The weights of the losses are $\lambda_{box} = 7.5$, $\lambda_{conf} = 1.5$ and $1e-7$ for λ_{syn} . Finally, we train our models with a batch size of 32, a sequence length of 64, and an initial learning rate of $1e-3$. The training takes 6 hour on a single NVIDIA GeForce RTX 4090. We evaluated our models on our proposed dataset. We tested our results by leaving one recording out without shuffling and averaging the results.

5.2. Ablation Studies

This section examines the two main components of our methodology: the dynamic event windows and the temporal weighted-sum filter. The ablation studies are performed on the Ini-30 Dataset and using the best models.

5.2.1 Model Components

Event Slicing Window: In Tab. 6, we evaluate the effects of fixed time windows (dt) on the precision of pupil localisation. The evaluation considers the median, the minimum and maximum number of events/time-window per bin, see Tab. 3. The comparison is carried out considering the average time window. The dynamic event time window consistently outperform the fixed time window on the validation set.

Temporal Weighted-Sum Filter The temporal weighted-sum filter plays a crucial role in enhancing the performance of our model. In Tab. 7, we present an evaluation of the impact of two key parameters, namely τ_{mem} and τ_{syn} , on the overall effectiveness of the filter. Notably, the without the filter yields an error of 24.46 pixels (± 3.17). Adjusting the values of τ_{mem} and τ_{syn} allows for a tailored optimization of the filter’s performance.

5.3. Benchmark Comparison

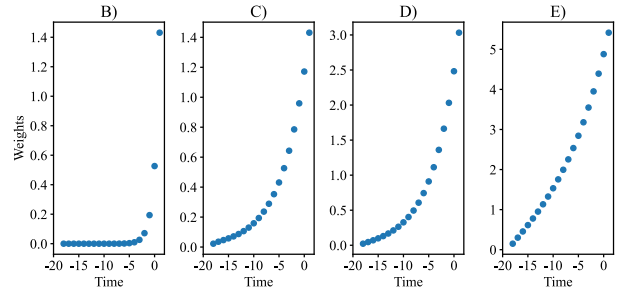
Centroid Error : We quantified the efficacy of our system using the Centroid Error metric. Additional experiments were conducted on variants of the Retina model, specifically one without neuron state resets (“Retina w/o resets”) and another trained with 3ET’s loss function (“Retina w/o

Table 6. The performance of different event slicing methods.

Method	Event Count	Time Window	Error (px) ↓
Fixed	198 [52, 401]	1.1ms	4.40 (± 2.69)
Dynamic	100	1.1ms [0.41, 3.1ms]	3.54 (± 1.43)
Fixed	242 [69, 481]	1.6ms	5.18 (± 1.37)
Dynamic	150	1.6ms [0.63, 4.0ms]	3.49 (± 1.18)
Fixed	277 [84, 541]	2.1ms	3.39 (± 1.02)
Dynamic	200	2.1ms [0.86, 4.6ms]	3.46 (± 1.36)
Fixed	331 [110, 630]	3.0ms	3.71 (± 1.40)
Dynamic	300	3.0ms [1.10, 8.4ms]	3.24 (± 0.79)

Table 7. The effect of the components of the temporal filter.

Figure	τ_{mem}	τ_{syn}	Kernel Size	Error (px) ↓
-	Not Used			24.46 (± 3.17)
B	5	1	20	21.70 (± 4.54)
C	1	5	20	8.72 (± 4.60)
D	5	5	20	3.24 (± 0.79)
E	10	10	20	3.52 (± 0.89)



box”). The latter variant shares the same network architecture as Retina, except for the output layer, which directly predicts pupil coordinates.

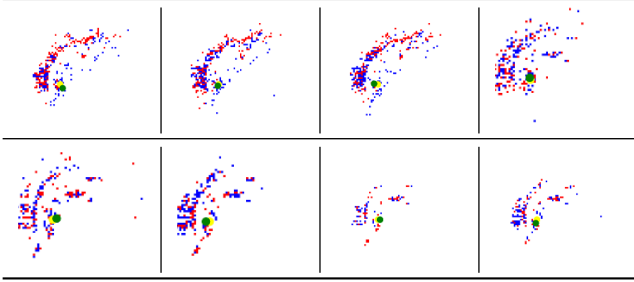
Tab. 8 presents the Centroid Error results for different DVS resolutions. The resolutions are set to 64x64x2 pixels. Notably, our Retina model outperforms 3ET [5] and the variants of Retina, achieving a significant reduction in Centroid Error to 3.24 (± 0.79) pixels.

The visualizations in Tab. 9 provide a qualitative insight into the model’s performance on samples from the valida-

Table 8. The performance of our model on the validation set.

Method	Input	Window	Error (px) ↓
3ET [5]	Events	Fixed (3ms)	4.48 (\pm 1.94)
Retina w/o <i>box</i>	Events	Dynamic (300)	5.89 (\pm 1.71)
Retina w/o <i>reset</i>	Events	Dynamic (300)	7.99 (\pm 5.79)
Retina	Events	Dynamic (300)	3.24 (\pm 0.79)

tion set using different time windows.

Table 9. The predictions (green) plotted with the target label (yellow) on samples from the validation set using a dynamic time window (row 1) and fixed time window (row 2).

Network Complexity: In Tab. 10, we present a comprehensive comparison between our proposed model and the state-of-the-art 3ET [5], focusing on both the number of parameters and the volume of MAC operations. Notably, our model demonstrates a remarkable reduction in complexity, underscoring its efficiency.

Table 10. A breakdown of the network complexity.

Method	MAC Operations ↓	Parameters ↓
3ET [5]	107M	418k
Retina w/o L_{box}	2.53M	43k
Retina	3.03M	63k

Latency & Power: In this section, we present a comprehensive analysis of the power consumption and latency metrics on the Speck platform. We evaluated two different time windows of events, namely the Dynamic Window (300 events) and the Fixed Window (3ms), to study the system’s performance under different event distributions. We injected the different bins at sufficiently distant timestamps (100ms) in order to isolate the response of the chip at every time bin. Tab. 11 provides an overview of the power consumption across various components contributing to the overall power profile in the Speck namely : Vdd, Vda, (referring to the digital and analog steps on the DVS), Logic (the power usage of the SNN), RAM, and I/O. The Dynamic event Window can be used to stabilize the power consumption in case higher rates of events are expected, however in

our test the Fixed Window was able to utilize the resources available more efficiently. We computed the latency by calculating the difference between the timestamp of a set of spikes (2500) for any given bin compared to the input timestamp. We averaged the different responses and obtained a total latency for the Dynamic Window of 8.01 ms and 5.57 ms for Fixed Window.

Table 11. The average and peak latency (L - ms) and power consumption (P - mW) on Speck for the validation dataset using two time windows of events.

Type	Name	Unit	Dynamic	Fixed
Sensor	Vdd	mW	0.03 [0.01-0.05]	
Sensor	Vda	mW	0.6 [0.58-0.63]	
Device	Logic	mW	2.43 [0.28-14.34]	1.26 [0.28-15.08]
Device	RAM	mW	1.64 [0.01-9.44]	0.90 [0.03-8.95]
Device	I/O	mW	0.10 [0.08-0.23]	
End-to-End	Total ↓	mW	4.80	2.89
End-to-End	Total ↓	mS	8.01	5.57
End-to-End	Total ↓	mJ	38.40	16.10

6. Discussion and Future Work

Our model experiences an accuracy decline when trained without the continuous resetting of neuron states. The ongoing reset of neuron states may introduce potential disruptions in continuous tracking on a neuromorphic chip, particularly if the reset frequency surpasses the internal clock frequency of the neuromorphic system. Exploring strategies to mitigate these challenges and optimize model performance under those additional hardware constraints is a promising avenue for future research.

7. Conclusion

Our work describes an energy-efficient (5mW, end-to-end), low latency (6ms, end-to-end), and accurate (3-4px) neuromorphic approach for eye tracking, leveraging the strengths of the neuromorphic form of both sensor and processor, and a truly lightweight and deployable spiking neural network model. The presented model demonstrates better than baseline precision with significantly reduced computational complexity. Finally, we hope the introduced event-based eye-tracking dataset could promote further exploration in the realm of real-world ultra-low power eye-tracking technology.

References

- [1] Anastasios N Angelopoulos, Julien NP Martel, Amit PS Kohli, Jorg Conradt, and Gordon Wetzstein. Event based, near eye gaze tracking beyond 10,000 hz. *IEEEVR*, 2020. 1, 3, 4
- [2] Sizhen Bian, Lukas Schulthess, Georg Rutishauser, Alfio Di Mauro, Luca Benini, and Michele Magno. Colibriuav: An ultra-fast, energy-efficient neuromorphic edge processing uav-platform with event-based and frame-based cameras. *arXiv preprint arXiv:2305.18371*, 2023. 1
- [3] Pietro Bonazzi, Thomas Rüegg, Sizhen Bian, Yawei Li, and Michele Magno. Tinytracker: Ultra-fast and ultra-low-power edge vision in-sensor for gaze estimation. *IEEE Sensors*, 2023. 2
- [4] Hannah Bos and Dylan Muir. Sub-mw neuromorphic snn audio processing applications with rockpool and xylo. *Embedded Artificial Intelligence: Devices, Embedded Systems, and Industrial Applications*, page 69, 2023. 1, 2
- [5] Qinyu Chen, Zuowen Wang, Shih-Chii Liu, and Chang Gao. 3et: Efficient event-based eye tracking using a change-based convlstm network. *arXiv preprint arXiv:2308.11771*, 2023. 1, 2, 3, 7, 8
- [6] Guillermo Gallego, Tobi Delbrück, Garrick Orchard, Chiara Bartolozzi, Brian Taba, Andrea Censi, Stefan Leutenegger, Andrew J. Davison, Jörg Conradt, Kostas Daniilidis, and Davide Scaramuzza. Event-based vision: A survey. *CoRR*, abs/1904.08405, 2019. 3
- [7] Jan Hendrik Hosang, Rodrigo Benenson, and Bernt Schiele. Learning non-maximum suppression. *CoRR*, abs/1705.02950, 2017. 5
- [8] Benedikt Hosp, Shahram Eivazi, Maximilian Maurer, Wolfgang Fuhl, David Geisler, and Enkelejda Kasneci. Remote-eye: An open-source high-speed remote eye tracker: Implementation insights of a pupil-and glint-detection algorithm for high-speed remote eye tracking. *Behavior research methods*, 52:1387–1401, 2020. 2
- [9] Petr Kellnhofer, Adria Recasens, Simon Stent, Wojciech Matusik, and Antonio Torralba. Gaze360: Physically unconstrained gaze estimation in the wild. In *Proceedings of the IEEE/CVF international conference on computer vision*, pages 6912–6921, 2019. 2
- [10] Muhammad Qasim Khan and Sukhan Lee. Gaze and eye tracking: Techniques and applications in adas. *Sensors*, 19(24):5540, 2019. 2
- [11] K. Krafska, A. Khosla, P. Kellnhofer, H. Kannan, S. Bhandarkar, W. Matusik, and A. Torralba. Eye tracking for everyone. In *IEEE Conference on Computer Vision and Pattern Recognition (CVPR)*, 2016. 3
- [12] Clara Mestre, Josselin Gautier, and Jaume Pujol. Robust eye tracking based on multiple corneal reflections for clinical applications. *Journal of biomedical optics*, 23(3):035001–035001, 2018. 2
- [13] Julian Moosmann, Pietro Bonazzi, Yawei Li, Sizhen Bian, Philipp Mayer, Luca Benini, and Michele Magno. Ultra-efficient on-device object detection on ai-integrated smart glasses with tinyssimoyolo, 2023. 2
- [14] Emre O. Neftci, Hesham Mostafa, and Friedemann Zenke. Surrogate gradient learning in spiking neural networks. *CoRR*, abs/1901.09948, 2019. 5
- [15] Cristina Palmero, Javier Selva, Mohammad Ali Bagheri, and Sergio Escalera. Recurrent cnn for 3d gaze estimation using appearance and shape cues. *arXiv preprint arXiv:1805.03064*, 2018. 2
- [16] Nitin Rath, Indranil Chakraborty, Adarsh Kosta, Abhronil Sengupta, Aayush Ankit, Priyadarshini Panda, and Kaushik Roy. Exploring neuromorphic computing based on spiking neural networks: Algorithms to hardware. *ACM Computing Surveys*, 55(12):1–49, 2023. 1
- [17] Joseph Redmon, Santosh Divvala, Ross Girshick, and Ali Farhadi. You only look once: Unified, real-time object detection, 2016. 5, 2
- [18] Georg Rutishauser, Robin Hunziker, Alfio Di Mauro, Sizhen Bian, Luca Benini, and Michele Magno. Colibries: A milliwatts risc-v based embedded system leveraging neuromorphic and neural networks hardware accelerators for low-latency closed-loop control applications. *arXiv preprint arXiv:2302.07957*, 2023. 1
- [19] Timo Stoffregen, Hossein Daraei, Clare Robinson, and Alexander Fix. Event-based kilohertz eye tracking using coded differential lighting. In *Proceedings of the IEEE/CVF Winter Conference on Applications of Computer Vision*, pages 2515–2523, 2022. 3
- [20] Engin Türetkin, Sareh Saeedi, Siavash Bigdeli, Patrick Stadelmann, Nicolas Cantale, Luis Lutnyk, Martin Raubal, and Andrea L Dunbar. Real time eye gaze tracking for human machine interaction in the cockpit. In *AI and Optical Data Sciences III*, pages 24–33. SPIE, 2022. 2
- [21] Kang Wang and Qiang Ji. Real time eye gaze tracking with 3d deformable eye-face model. In *Proceedings of the IEEE International Conference on Computer Vision*, pages 1003–1011, 2017. 2
- [22] Philipp Weidel and Sadique Sheik. Wavesense: Efficient temporal convolutions with spiking neural networks for keyword spotting, 2021. 5
- [23] Ruohan Zhang, Zhuode Liu, Luxin Zhang, Jake A Whritner, Karl S Muller, Mary M Hayhoe, and Dana H Ballard. Agil: Learning attention for human for visuomotor tasks. In *Proceedings of the European Conference on Computer Vision (ECCV)*, pages 663–679, 2018. 3
- [24] Xucong Zhang, Yusuke Sugano, and Andreas Bulling. Evaluation of appearance-based methods and implications for gaze-based applications. In *Proceedings of the 2019 CHI conference on human factors in computing systems*, pages 1–13, 2019. 1, 2
- [25] Guangrong Zhao, Yurun Yang, Jingwei Liu, Ning Chen, Yiran Shen, Hongkai Wen, and Guohao Lan. Ev-eye: Rethinking high-frequency eye tracking through the lenses of event cameras. In *Thirty-seventh Conference on Neural Information Processing Systems Datasets and Benchmarks Track*, 2023. 1, 3, 4

A Low-Power Neuromorphic Approach for Efficient Eye-Tracking

Supplementary Material

We provide illustrative graphs for the processes behind dynamic time window slicing (Listing 1) and the temporal weighted-sum filter Fig. 4. In addition, we include background information regarding the IAF neuron model (Sec. B) and the hardware (Sec. C). Furthermore, in Sec. D we study the firing rate of different time window methods. Finally, Sec. E provides a benchmark for future work on eye detection on Ini-30 in terms of centroid error, power consumption and latency.

A. Dynamic Time Window

For better illustration, in Listing 1, we illustrate the operating principles and code to slice events into windows of dynamic time lengths.

```

1 # data preparation
2 import numpy as np
3 XYP=last_events_before_pupil_label
4 end_index = len(XYP) - 1
5 # event bins
6 tcwh=np.zeros(64,2,64,64)
7 for i in reversed(range(64)):
8     # events for time bin (i)
9     x,y=last_unique_evs(XYP[:end_index,:2],N)
10    start_index=end_index-len(x)
11    p=XYP[start_index:end_index]
12    # add events for i
13    np.add.at(tcwh[i,0], (x[p==0],y[p==0]),1)
14    np.add.at(tcwh[i,1], (x[p==1],y[p==1]),1)
15    # recover 1-bit event channel
16    tcwh[i,0][tcwh[i,1]>=tcwh[i,0]]=0
17    tcwh[i,1][tcwh[i,1]<tcwh[i,0]]=0
18    tcwh[i]=tcwh[i].clip(0, 1)
19    # move index
20    end_index = start_index

```

Listing 1. The code to dynamically slice event windows in time

B. Neuron Models

The IAF neuron model, operating after every convolution layer, is characterized by a straightforward mathematical formulation. It involves the integration of incoming synaptic inputs (convolution operations) and the generation of a spike once a certain membrane potential threshold is reached. The dynamics of the IAF neuron are described by the following differential equation:

$$\tau_m \frac{dV}{dt} = -V(t) + R_m I_{syn}(t) \quad (8)$$

where $V(t)$ is the membrane potential at time t , τ_m is the membrane time constant, R_m is the membrane resistance, and $I_{syn}(t)$ represents the synaptic input current. The neuron fires when $V(t)$ surpasses a predefined threshold $V(th) = 1$, at which point the membrane potential is reset to a resting value $V(reset) = 0$. One of the key features

of the IAF neuron model is its integration mechanism for incoming synaptic inputs. The synaptic input $I_{syn}(t)$ is often modeled as a sum of weighted contributions from different synapses:

$$I_{syn}(t) = \sum_j w_j \cdot I_j(t - t_j) \quad (9)$$

where w_j represents the synaptic weight, $I_j(t - t_j)$ is the synaptic input spike train arriving at time t from synapse j with a spike at t_j .

C. Hardware Description

Speck is equipped with nine cores with different kernel and neuron memory limitations, see Tab. 12.

Table 12. The memory limits of each core in Speck are reported in kibibyte (1 Ki = 1024 bytes).

Core ID	K_{MT} (Ki)	N_M (Ki)
0	16	64
1	16	64
2	16	64
3	32	32
4	32	32
5	64	16
6	64	16
7	16	16
8	16	16

D. Firing Rate

In Fig. 5, we provide insights into the firing behavior of the SNN at different network depths. Results show the dynamic time window of events has considerably lower firing rate in the first layer. For the rest of the layers, there is no significant variation between the spiking activity across different slicing methods, different time window or different event counts.

At the beginning, the network can save energy consumption by having less than 30% spikes generated per layer. The higher firing rates at the ends might be the results of directly converting spikes to bounding boxes coordinates $[0,1]$.

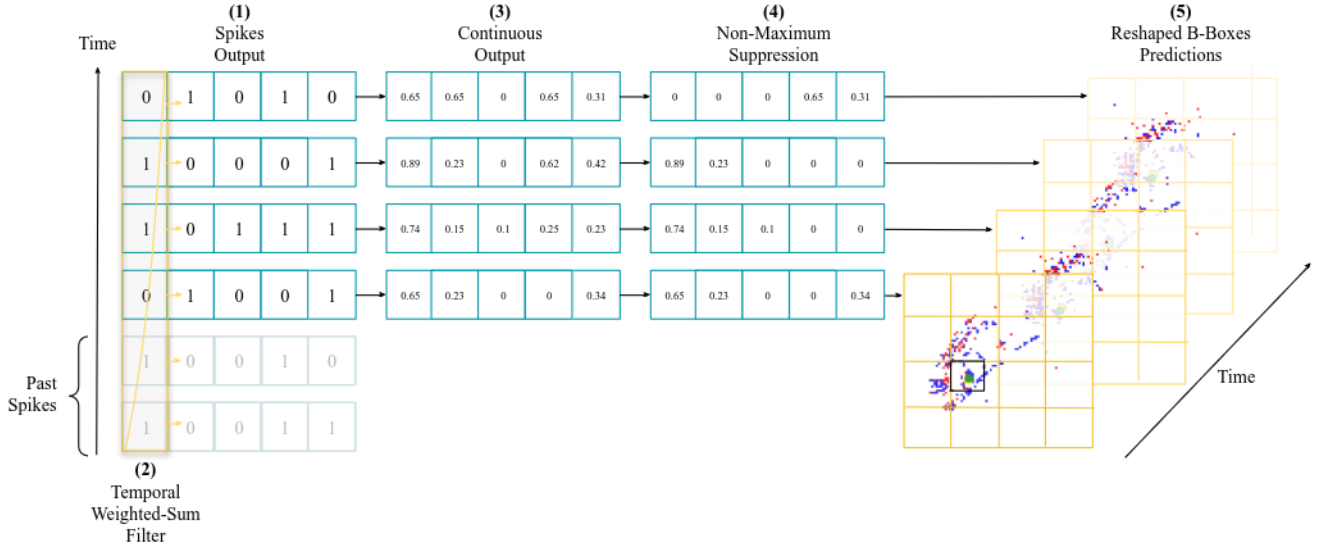


Figure 4. Overview of the steps involved in the conversion of spikes to bounding boxes. The output spikes 1) are multiplied to a temporal weighted sum filter 2). Next, only during training, the continuous output 3) is zeroed in cells where bounding boxes were non-existent in the target 4). Finally the centroid of the predicted bounding box is used to find the coordinate of the pupil 5).

E. Additional Results

E.1. Benchmark Eye Detection on Ini-30

In this section material, we consider the simpler task of eye detection and provide two benchmarks for future work on Ini-30.

E.1.1 Eye Detection Architectures

For pupil detection, we evaluate models which do not possess a temporal dimension. In this task, we evaluate a standard Convolutional Neuron Network (CNN) and compared it with an edge-version of the yolo network [17], namely Tinyissimo-YoloV8 (TY-V8) [13], which has been proven to be well-suited for deployment on ultra-low power micro-controllers. Since pupil detection has only one class we reduced the depth multiple in [13] to 0.1 (versus 0.3), the layer channel multiple of 0.1 (versus 0.18), reduced the number of predictions heads from 16 to 1 and thus obtained a model of around 30k parameters (vs 1M for Tinyissimo-YoloV8-B). In these experiments, we accumulated events with linear decay with time windows of 3ms.

E.1.2 Centroid Error

In Tab. 13, we evaluate the efficiency of these models in terms of number of MAC and parameters and report the centroid error on the validation set after 520k steps. The CNN was trained with the original resolution and showed an error of 5px. In relative terms (RError), this corresponds

to 0.5px in the 64x64 array. TY-V8 was instead trained on a 128x128 resolution and resulted in a 3.5px error (1.75px in 64x64). Both of these models are relative more precise than Retina, however neither of these architectures can be deployed on neuromorphic hardware.

Table 13. The benchmark for network complexity and error for pupil detection (64x64).

Model	MAC (M) ↓	Params (k) ↓	Error (px) ↓
CNN (Baseline)	150	120	0.5
TY-V8	0.42	28	1.75

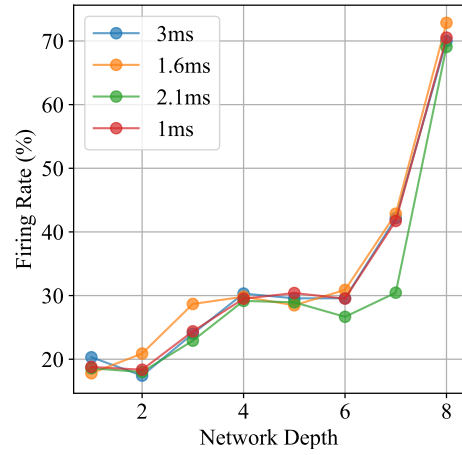
E.1.3 Latency & Power

In Tab. 11, we evaluate the power consumption of the eye detection models on two processors. We deployed the first large CNN on an Intel® Core™ i7 Processor and the second TY-V8 on the GAP9 RISC-V Processor from GreenWaves.

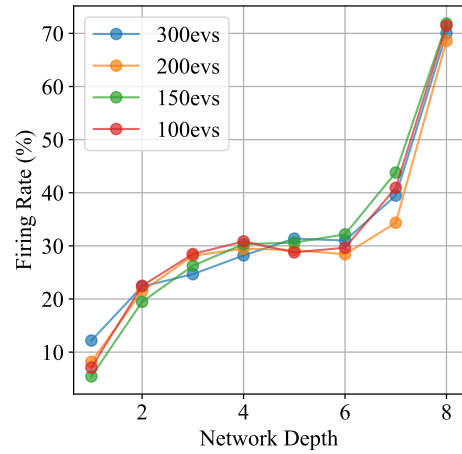
Table 14. The benchmark for latency (mS) and power (mW) for pupil detection.

Model	Platform	Latency [ms] ↓	Power ↓
CNN (Baseline)	i7 CPU	3.0	225 W
TY-V8	GAP9	6.1	94 mW

Our results indicates higher power consumption (in particular in i7) and comparable latency w.r.t. Speck.



(a) Firing Rates of the Fixed Time Window.



(b) Firing Rates of the Dynamic Time Window.

Figure 5. The firing rates of the trained SNN at different network depths with different slicing methods and time windows.